Simulated winter circulation types in the North Atlantic and European region for preindustrial and glacial conditions

D. Hofer,[1,2] C. C. Raible,[1,2] N. Merz,[1,2] A. Dehnert,[3] and J. Kuhlemann[3]

Received 9 May 2012; revised 25 June 2012; accepted 25 June 2012; published 7 August 2012.

[1] Winter circulation types under preindustrial and glacial conditions are investigated and used to quantify their impact on precipitation. The analysis is based on daily mean sea level pressure fields of a highly resolved atmospheric general circulation model and focuses on the North Atlantic and European region. We find that glacial circulation types are dominated by patterns with an east-west pressure gradient, which clearly differs from the predominantly zonal patterns for the recent past. This is also evident in the frequency of occurrence of circulation types when projecting preindustrial circulation types onto the glacial simulations. The elevation of the Laurentide ice sheet is identified as a major cause for these differences. In areas of strong precipitation signals in glacial times, the changes in the frequencies of occurrence of the circulation types explain up to 60% of the total difference between preindustrial and glacial simulations. **Citation:** Hofer, D., C. C. Raible, N. Merz, A. Dehnert, and J. Kuhlemann (2012), Simulated winter circulation types in the North Atlantic and European region for preindustrial and glacial conditions, *Geophys. Res. Lett.*, *39*, L15805, doi:10.1029/2012GL052296.

1. Introduction

[2] For the North Atlantic region, model simulations of the Last Glacial Maximum (LGM, around 21,000 years before present) exhibit major differences in the atmospheric dynamics compared with today that are mostly attributed to changes in the topography [e.g., *Kutzbach and Guetter*, 1986; *Kageyama and Valdes*, 2000; *Pausata et al.*, 2011; *Hofer et al.*, 2012]. A robust feature of LGM winter (December to February, DJF) circulation in model simulations is a southward displacement of the high and low pressure centers and a southeastward shift of the storm tracks [*Laîné et al.*, 2009; *Pausata et al.*, 2011]. Associated with these changes is an increase of precipitation in the mid-latitudes especially around the Iberian Peninsula that overcompensates the general drying due to reduced evaporation as the temperature is lower [*Laîné et al.*, 2009; *Strandberg et al.*, 2011; *Hofer et al.*, 2012].

[3] In this study, we use circulation type classification based on a k-means clustering algorithm [*Huth et al.*, 2008] to analyze the changes in the atmospheric dynamics and to quantify its contribution to the precipitation changes for different glacial boundary conditions. Circulation type classification allows more insights than an analysis of the mean changes not only in how the atmospheric circulation is changed in glacial states, but also connects these changes to regional and local weather. It has widely been used for observations and model data of the recent past and for future projections [*Huth et al.*, 2008, and references therein]. In contrast, its application to glacial simulations is rare. Based on one such analysis *Kageyama et al.* [1999] concluded that due to large changes in the boundary conditions no circulation regimes can be identified in the North Atlantic region for LGM and that present-day circulation regimes are irrelevant for LGM, i.e., they can not be projected onto the glacial circulation. However, the analysis is based on an atmosphere general circulation model with a low spatial resolution compared with current models. As shown by *Unterman et al.* [2011], a higher spatial and temporal resolution allows additional insights into LGM dynamics. Thus, a reexamination of the results of *Kageyama et al.* [1999] using an up-to-date model seems appropriated. In addition, we extend the analysis to an earlier glacial state at 65,000 years before present (Marine Isotope Stage 4; MIS4) where different ice sheet topographies are applied. On the one hand, the ice sheet topography in MIS4 is more uncertain and therefore we apply different scenarios, and, on the other hand, the different scenarios allow to gain further insights of the impact of topographic changes on atmospheric dynamics and the associated changes in precipitation. Besides, by using two states of the last glaciation the effect of other boundary conditions can be quantified and put into perspective to the topographic impact.

2. Data and Methods

[4] This study uses the Community Climate System Model version 4 (CCSM4; provided by the National Center of Atmospheric Research) in a horizontal resolution of $0.9° \times 1.25°$ [*Gent et al.*, 2011]. The model is run with an interactive atmosphere and land surface, while time-varying sea ice cover and sea surface temperatures (SSTs) are prescribed based on simulations with the lower-resolved, but fully coupled CCSM3. For each time period investigated (recent past, LGM, and MIS4) an equilibrium CCSM3 simulation has been conducted and the monthly means of the SST and sea ice cover fields of the last few decades of the simulation are used as lower boundary forcing for the CCSM4 simulations of the corresponding time period (see *Hofer et al.* [2012] for further information on the CCSM3 simulations). Thus, the ocean surface forcing also includes interannual variability.

[1]Climate and Environmental Physics, Physics Institute, University of Bern, Bern, Switzerland.
[2]Oeschger Centre for Climate Change Research, University of Bern, Bern, Switzerland.
[3]Swiss Federal Nuclear Safety Inspectorate, Brugg, Switzerland.

Corresponding author: D. Hofer, Climate and Environmental Physics, Physics Institute, University of Bern, Sidlerstrasse 5, CH-3012 Bern, Switzerland. (dhofer@climate.unibe.ch)

0094-8276/12/2012GL052296

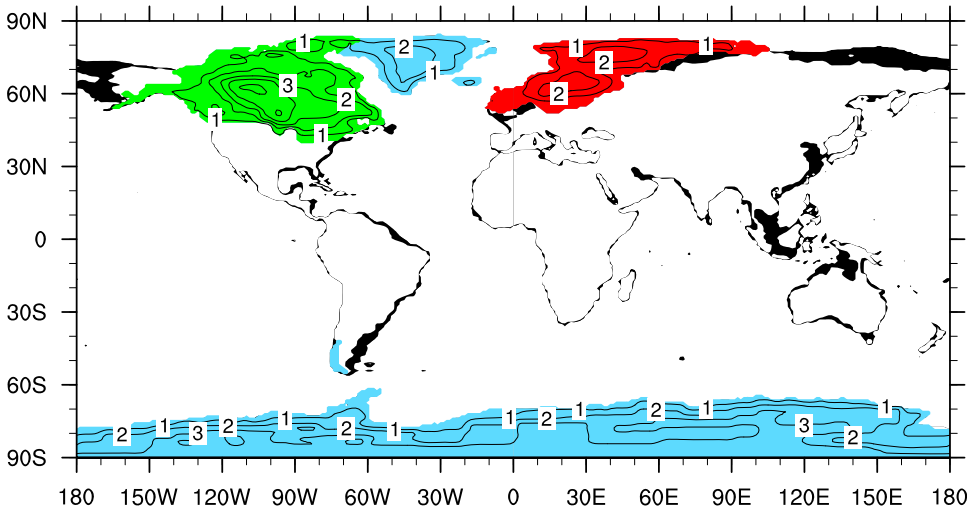

Figure 1. LGM ice sheet extent (light blue for Greenland and Antarctica, green for the Laurentide ice sheet, and red for the Fennoscandian ice sheet) and thickness (contours, interval 1 km), and additional land areas (black; shown as the boundary of 50% land fraction) due to the sea-level decrease of 120 m with respect to today. The coastlines and ice sheets are based on ICE-5G [*Peltier*, 2004].

[5] A preindustrial simulation (1850 AD; hereafter PI) that serves as reference simulation and five glacial experiments have been conducted under different forcing conditions for 33 model years; the analysis is based on the last 30 model years. The boundary conditions of the PI simulation are presented in *Gent et al.* [2011]. In one glacial simulation LGM boundary condition are applied: lower concentrations of greenhouse gases (CO_2 = 185 ppm; N_2O = 200 ppb; CH_4 = 350 ppb), changed Earth's orbital parameters (calculated according to *Berger* [1978]), added major continental ice sheets [*Peltier*, 2004], and sea level that is 120 m lower than today (Figure 1). The other four glacial simulations use conditions according to 65,000 years before present (CO_2 = 205 ppm; N_2O = 210 ppb; CH_4 = 460 ppb; adjusted Earth's orbital parameters; 80 m lower sea level than today) with different ice sheet topographies. In all four simulations the spatial extent of the ice sheets is similar as in LGM, but their elevation is adjusted individually (see Figure 1 for the exact regions): (i) linear distribution with 67% of the LGM height ($MIS4_{LIN}$), (ii) lower Fennoscandian ice sheet (33% of the LGM height and 74% elsewhere; $MIS4_{FS}$) (iii) lower Laurentide ice sheet (46% of the LGM height and 100% elsewhere; $MIS4_{LT}$), and (iv) full LGM heights everywhere ($MIS4_{LGM}$).

[6] To identify the circulation types in the simulations, the k-means clustering algorithm is applied to the 20 leading principal components (which explain 93%–95% of the variance) of daily means of the winter sea level pressure (SLP) in the North Atlantic region (25°N–70°N and 70°W–50°E). As the algorithm can end up in a local minimum, the clustering is repeated 1000 times with different initial seed partitions. The number of clusters is varied from 2 to 15 and the separability among the circulation types and the within-type variability are estimated using different metrics (explained variation, pseudo-F statistic and Silhouette index [*Huth et al.*, 2008]) to identify the optimal number of clusters. However, the results are generally not unequivocal, pointing to an optimal number between 6 and 9. Thus, the analysis is performed with 6 to 9 clusters and – as the main conclusions are similar – only the results for 6 clusters are shown. For such numbers of clusters, the explained variations [*Huth et al.*, 2008] in PI and in the glacial experiments are similar, which suggests that it is reasonable to apply the circulation type classification to both. Note that the results do not depend strongly on the region chosen as slightly shifted boundaries lead to the same main conclusions.

[7] The circulation type patterns of the different simulations are compared by calculating their spatial correlations and the projected frequencies of occurrence. To estimate the latter, for each day of a simulation the spatial correlation coefficients between the daily mean SLP pattern and the different circulation type patterns are calculated. The day is then assigned to the circulation type with which it has the maximum spatial correlation coefficient. The frequency of occurrence is the number of days that are associated with a circulation type.

3. Circulation Types

[8] For present-day conditions the circulation type patterns in the model reasonably agree with the ones derived from reanalysis data (ERA-40 [*Uppala et al.*, 2005]) and also exhibit high spatial correlation coefficients (>0.85) with the patterns of the PI simulation (not shown). For PI zonal SLP patterns prevail (Figure 2a). The three most frequent circulation type patterns for PI (Figure 2a, patterns 1–3) show a strong meridional SLP gradient, while only the least frequent circulation type (Figure 2a, pattern 6) exhibits a pronounced east-west pressure difference. The circulation type patterns in the glacial simulations are clearly different with a distinct negative SLP anomaly west to northwest of the British Isles (e.g., Figure 2c for $MIS4_{LGM}$). While some glacial circulation types resemble the ones of PI (the one matching best is pattern 4, which has a spatial correlation coefficient of 0.92 with pattern 2 of PI) for others no good correspondence is found (for pattern 3 the highest spatial correlation is 0.58 with pattern 6 of PI). Generally, the deviations to PI are larger in the simulations where the

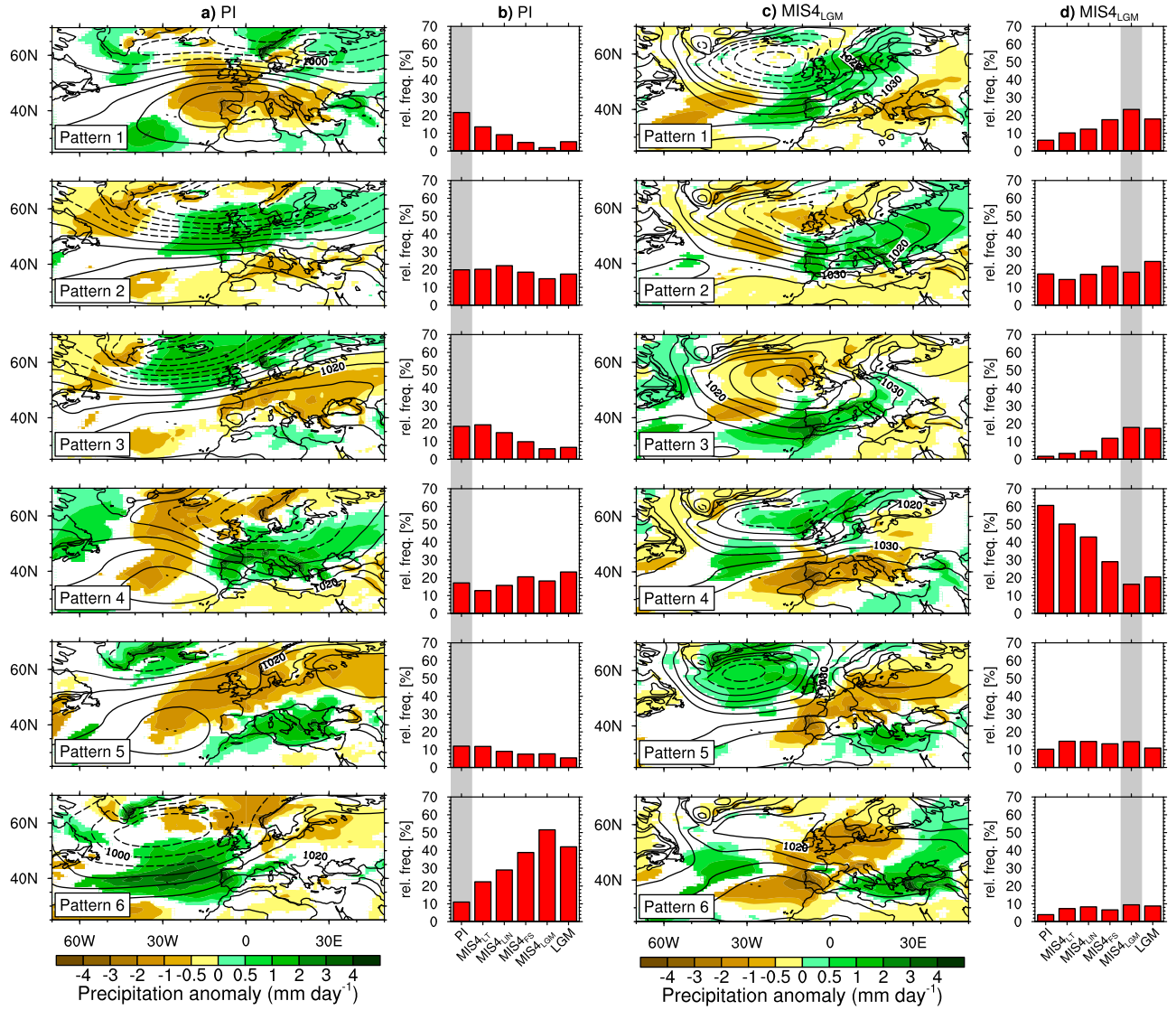

Figure 2. The six patterns (contours) and the associated precipitation anomalies (color shading) for the circulation types in winter (DJF) of (a) the PI and (c) the $MIS4_{LGM}$ simulations obtained by the k-means cluster analysis of the 20 leading principal components of daily SLP fields, and their projected frequencies in all simulations (b) for PI and (d) for $MIS4_{LGM}$. The circulation type patterns are arranged from top to bottom according to their frequency of occurrence. The contour interval is 5 hPa with a bold line at 1010 hPa and continuous (dashed) lines indicating values above (below) 1010 hPa. The precipitation anomalies are calculated as the difference between the mean precipitation of all days that are assigned to a circulation type pattern and the overall winter mean precipitation and only values that are statistically significant at the 5% level based on the two-sided Student's *t* test are colored. The frequencies of occurrence are calculated as the sum of all days where the daily mean SLP pattern of a simulation has the highest spatial correlation with this circulation type pattern divided by the total sum of days (in %). The gray shading highlights the simulation from where the circulation type patterns originate. The MIS4 simulations (in Figures 2b and 2d) are arranged from left to right in the order of increasing height of the Laurentide ice sheet.

Laurentide ice sheet is more elevated. Thus, strong topographic changes associated with the large continental ice sheets lead to strongly different circulation types in glacial periods compared with today.

[9] Nevertheless and in contrast to *Kageyama et al.* [1999], it is possible to project the preindustrial circulation types on glacial simulations (and vice versa), via spatial correlation as discussed in Sect. 2. In doing so, SLP composites in the glacial simulations resemble the preindustrial circulation types. In any case, the spatial correlation coefficients between the two are >0.8 and most of them are >0.9. The analysis shows that the projected frequencies of occurrence confirm the aforementioned impact of the topography (Figures 2b and 2d). Considering the patterns derived from PI, the projections of pattern 1 and 6 (to a lesser degree also the one of pattern 3) change in accordance with the elevation of the Laurentide ice sheet. Pattern 1 occurs less often in the glacial simulations, while pattern 6 represents the dominant glacial circulation pattern and thus its frequency of occurrence increases with increasing topography. This is

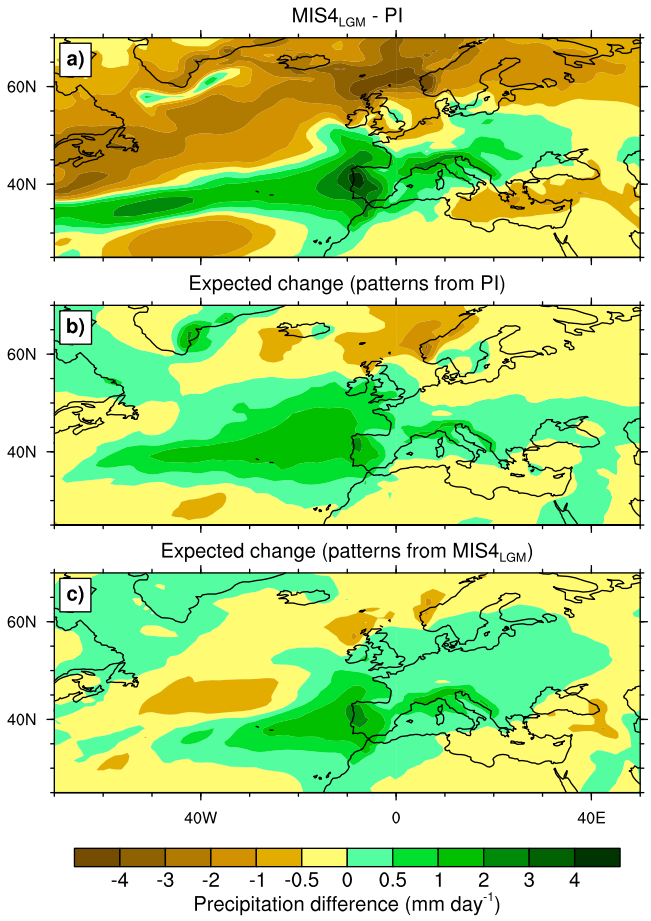

Figure 3. Winter (DJF) precipitation: (a) difference between the mean precipitation in the $MIS4_{LGM}$ and the PI simulations, (b) expected difference due to the changed frequencies of occurrence of the SLP patterns using the precipitation anomalies estimated from the PI simulation (see text for details on the calculation), and (c) same as Figure 3b but using the precipitation anomalies estimated from $MIS4_{LGM}$.

consistent with the comparison of the circulation types, namely that in the glacial simulations east-west SLP pattern prevail and not north-south as in the recent past, and that the main factor for the changes is the elevation of the Laurentide ice sheet. The reverse approach – using the projections based on the $MIS4_{LGM}$ circulation types – confirms the results. The first and third glacial circulation types rarely occur in PI and instead the forth, which is the only glacial type with a pronounced meridional SLP gradient, is much more frequent.

[10] The projected frequencies of occurrence for the LGM simulation are close to the ones for $MIS4_{LGM}$ suggesting a much weaker impact of other boundary conditions compared with topography.

4. Implications on Precipitation

[11] Each circulation type produces a specific precipitation pattern, which is calculated as the precipitation composite of all days that are associated with this type minus the mean precipitation (Figures 2a and 2c). By multiplying the obtained anomaly patterns with the relative change of their frequency of occurrence between two simulations, the contribution of circulation changes to precipitation changes is estimated.

[12] Figure 3a shows the mean precipitation difference between $MIS4_{LGM}$ and the PI simulation with a reduction in the northern North Atlantic and a band of increased precipitation in the mid-latitudes (from the eastern coast of North America to southeastern Europe). The expected differences due to the changes of the frequencies of occurrence of the circulation types are presented in Figures 3b and 3c. They are calculated using either the precipitation anomaly patterns from the PI simulation (Figure 3b) or the ones that are estimated when the preindustrial patterns are projected to MIS_{LGM} (Figure 3c). The most pronounced feature of the two patterns of the expected changes is a precipitation increase in the mid-latitudes. As for the mean difference the maximum precipitation increase is located over the Iberian Peninsula, but the positive anomalies extend too far to the North and are too sparse in the western part. Generally, the amplitudes of the expected changes are weaker than the ones of the mean difference. For Southwestern Europe and the adjacent ocean where the strongest precipitation increase is found in the glacial simulations, the expected changes can explain roughly 40% of the mean difference using the precipitation anomaly patterns from the PI simulation and 60% when the glacial anomaly patterns are used. In the glacial simulations with a less elevated Laurentide ice sheet the area of increased precipitation is reduced to the Iberian Peninsula (not shown). There, the explained percentage due to the changed frequencies of occurrence remains the same as in $MIS4_{LGM}$.

[13] The precipitation differences that can not be explained by circulation changes are in good agreement with the evaporation differences (Figure 4). In particular the northern and western regions are dominated by the impact of the evaporation change.

5. Conclusions

[14] Circulation type classification is used to investigate the differences between the glacial and the preindustrial climate. In contrast to the results of *Kageyama et al.* [1999], we find that DJF circulation types are present in glacial simulations and that the preindustrial circulation types can be projected in the glacial simulations. Our results suggest that the circulation types strongly differ under glacial boundary conditions compared with today, especially due to

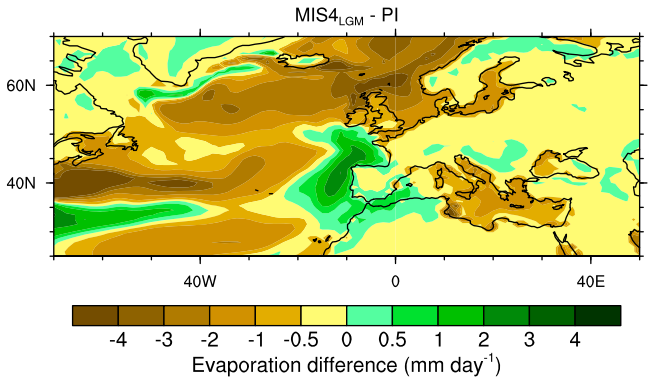

Figure 4. Difference of the evaporation rate between the $MIS4_{LGM}$ and the PI simulations.

the changed topography. This is consistent with other studies analyzing changes in atmospheric dynamics in the North Atlantic region [*Pausata et al.*, 2011; *Hofer et al.*, 2012]. It also resembles the findings by *Rivière et al.* [2010], who suggests the eddy-driven jet of the North Atlantic being North-South displaced in the PI, whereas it varies meridionally during LGM-like conditions. Also for the projections of the circulation types the surface elevation of the Laurentide ice sheet plays an important role. In the PI simulation circulation types with a north-south SLP gradient are dominant, while patterns with an east-west SLP gradient get more frequent with increasing elevation of the Laurentide ice sheet.

[15] Using the precipitation anomaly patterns that are associated with each circulation type the changed frequencies of occurrence can be transformed into precipitation changes. Our analysis shows evidences that the circulation changes can explain about 60% of the precipitation differences between the PI and the glacial simulations in areas (Southwestern Europe) where the strongest precipitation change is found. The remaining precipitation changes can be attributed to changes in evaporation.

[16] **Acknowledgments.** This work is funded by the Swiss Federal Nuclear Safety Inspectorate (ENSI). CCR is supported by the NCCR Climate. NM is founded by the EU project Past4Future from the European Commission's 7th Framework Programme (grant 243908; 2010–2014). Most simulations were performed at the Swiss National Supercomputing Centre (CSCS) in Manno. Some simulations and model data were kindly made available by the NCAR and by Jenny Brandefelt.

[17] The Editor thanks the two anonymous reviewers for assisting in the evaluation of this paper.

References

Berger, A. L. (1978), Long-term variations of daily insolation and quaternary climatic changes, *J. Atmos. Sci.*, *35*, 2362–2367.

Gent, P. R., et al. (2011), The Community Climate System Model Version 4, *J. Clim.*, *24*(19), 4973–4991, doi:10.1175/2011JCLI4083.1.

Hofer, D., C. C. Raible, A. Dehnert, and J. Kuhlemann (2012), The impact of different glacial boundary conditions on atmospheric dynamics and precipitation in the North Atlantic region, *Clim. Past*, *8*(3), 935–949, doi:10.5194/cp-8-935-2012.

Huth, R., C. Beck, A. Philipp, M. Demuzere, Z. Ustrnul, M. Cahynova, J. Kysely, and O. E. Tveito (2008), Classifications of atmospheric circulation patterns: Recent advances and applications, *Ann. N. Y. Acad. Sci.*, *1146*, 105–152, doi:10.1196/annals.1446.019.

Kageyama, M., and P. J. Valdes (2000), Impact of the North American ice-sheet orography on the Last Glacial Maximum eddies and snowfall, *Geophys. Res. Lett.*, *27*(10), 1515–1518, doi:10.1029/1999GL011274.

Kageyama, M., F. D'Andrea, G. Ramstein, P. J. Valdes, and R. Vautard (1999), Weather regimes in past climate atmospheric general circulation model simulations, *Clim. Dyn.*, *15*(10), 773–793.

Kutzbach, J. E., and P. J. Guetter (1986), The influence of changing orbital parameters and surface boundary-conditions on climate simulations for the past 18000 years, *J. Atmos. Sci.*, *43*(16), 1726–1759.

Laîné, A., M. Kageyama, D. Salas-Melia, A. Voldoire, G. Riviere, G. Ramstein, S. Planton, S. Tyteca, and J. Y. Peterschmitt (2009), Northern Hemisphere storm tracks during the Last Glacial Maximum in the PMIP2 ocean-atmosphere coupled models: Energetic study, seasonal cycle, precipitation, *Clim. Dyn.*, *32*(5), 593–614, doi:10.1007/s00382-008-0391-9.

Pausata, F. S. R., C. Li, J. J. Wettstein, M. Kageyama, and K. H. Nisancioglu (2011), The key role of topography in altering North Atlantic atmospheric circulation during the last glacial period, *Clim. Past*, *7*(4), 1089–1101, doi:10.5194/cp-7-1089-2011.

Peltier, W. R. (2004), Global glacial isostasy and the surface of the ice-age Earth: The ICE-5G (VM2) model and GRACE, *Annu. Rev. Earth Planet. Sci.*, *32*, 111–149.

Rivière, G., A. Laîné, G. Lapeyre, D. Salas-Melia, and M. Kageyama (2010), Links between rossby wave breaking and the North Atlantic oscillation-Arctic oscillation in present-day and Last Glacial Maximum climate simulations, *J. Clim.*, *23*(11), 2987–3008, doi:10.1175/2010JCLI3372.1.

Strandberg, G., J. Brandefelt, E. Kjellstrom, and B. Smith (2011), High-resolution regional simulation of Last Glacial Maximum climate in Europe, *Tellus, Ser. A*, *63*(1), 107–125, doi:10.1111/j.1600-0870.2010.00485.x.

Unterman, M. B., T. J. Crowley, K. I. Hodges, S.-J. Kim, and D. J. Erickson (2011), Paleometeorology: High resolution Northern Hemisphere wintertime mid-latitude dynamics during the Last Glacial Maximum, *Geophys. Res. Lett.*, *38*, L23702, doi:10.1029/2011GL049599.

Uppala, S. M., et al. (2005), The ERA-40 re-analysis, *Q. J. R. Meteorol. Soc.*, *131*(612), 2961–3012, doi:10.1256/qj.04.176.